Atmos. Chem. Phys. Discuss., 13, 32885–32923, 2013
www.atmos-chem-phys-discuss.net/13/32885/2013/
doi:10.5194/acpd-13-32885-2013

Atmospheric Chemistry and Physics Discussions

Modeling the influences of aerosols on pre-monsoon circulation and rainfall over Southeast Asia

D. Lee[1,2,3], Y. C. Sud[2], L. Oreopoulos[2], K.-M. Kim[2], W. K. Lau[2], and I.-S. Kang[3]

[1]GESTAR, Morgan State University, Baltimore, Maryland, USA
[2]Earth Sciences Division, NASA Goddard Space Flight Center, Greenbelt, Maryland, USA
[3]School of Earth and Environmental Sciences, Seoul National University, Seoul, South Korea

Received: 30 October 2013 – Accepted: 28 November 2013 – Published: 16 December 2013

Correspondence to: D. Lee (dongmin.lee@nasa.gov)

Published by Copernicus Publications on behalf of the European Geosciences Union.

Abstract

We conduct several sets of simulations with a version of the GEOS-5 Atmospheric Global Climate Model (AGCM) equipped with a two-moment cloud microphysical scheme to understand the role of biomass burning (BB) aerosol emissions in Southeast (SE) Asia in the pre-monsoon period February–May. Our experiments are designed so that both direct and indirect aerosol effects can be evaluated. For climatologically prescribed monthly sea surface temperatures, we conduct sets of model integrations with and without biomass burning emissions in the area of peak burning activity, and with direct aerosol radiative effects either active or deactivated. Taking appropriate differences between AGCM experiment sets we find that BB aerosols affect liquid clouds in statistically significantly ways, increasing cloud droplet number concentrations, decreasing droplet effective radii (i.e., a classic aerosol indirect effect), and locally suppressing precipitation due to a decelerate of the autoconversion process, with the latter effect apparently also leading to cloud condensate increases. Geographical re-arrangements of precipitation patterns, with precipitation increases downwind of aerosol sources are also seen, most likely because of advection of weakly precipitating cloud fields. Somewhat unexpectedly, the change in cloud radiative effects (cloud forcing) is in the direction of less cooling because of decreases in cloud fraction. Overall, however, because of direct radiative effect contributions, aerosols exert a negative forcing at both the top of the atmosphere and, perhaps most importantly, the surface, where decreased evaporation triggers feedbacks that further reduce precipitation. Invoking the approximation that direct and indirect aerosol effects are additive, we estimate that the overall precipitation reduction is about 40 % due to the direct effects of absorbing aerosols which stabilize the atmosphere and reduce surface latent heat fluxes via cooler land surface temperatures. Further refinements of our two-moment cloud microphysics scheme are needed for a more complete examination of the role of aerosol-convection interactions in the seasonal development of the SE Asia monsoon.

ACPD
13, 32885–32923, 2013

1 Introduction

Use of fossil fuels for ever-growing energy demands, particularly in developing countries, has led to increased concentrations of aerosol-laden combustion by-products, especially in the planetary boundary layer (PBL) (Roelofs, 2013). Moorthy et al. (2013) estimate that aerosols over India have been increasing at the rate of 2–4 % per year over the last three decades resulting in doubled aerosol optical depth (AOD) in India's lower atmosphere. Similar changes are expected over other regions such as South-East Asia (SEA). Biomass burning (BB) is an age-old method of disposing off the agricultural trash (Taylor, 2010) and in SEA occurs primarily during the spring season (i.e., February-March-April (FMA); Gautam et al., 2013). Some smoke is also released throughout the year when urban trash is burned, but without an urban sprawl as large as Mexico City (Li et al., 2012), this source is much smaller than springtime agricultural BB. Over SEA, the combustion by-products released into the atmosphere contain large quantities of biogenic aerosol/carbon particles whose quantitative estimates are being tabulated with extensive measurements (Wiedinmyer et al., 2011).

Biomass burning aerosols (BBA) absorb and reflect solar radiation, thereby reducing the solar radiation reaching the surface, reducing surface sensible and latent heat fluxes and in turn inhibiting both dry and moist convection (Twomey, 1977; IPCC, 2007; Sect. 7.5.3). On the other hand, absorption of solar radiation at the aerosol level warms the local atmosphere, inducing elevated heating that can invigorate air mass convergence near the surface and with the addition of sensible and latent heat, can make the PBL unstable enough to promote moist convection (Lau and Kim, 2013). The net outcome of the resulting complex feedback interactions may either increase or decrease local rainfall. Furthermore, many black carbon aerosols, after becoming impregnated with dilute acid in the humid environment, transform from hydrophobic to hydrophilic that can activate as CCNs. Hence more BBA lead to more CCN and eventually to more cloud particles. If we assume that the net condensate production is solely governed by cloud-scale dynamics, more CCN activation would imply smaller cloud particles and

ACPD
13, 32885–32923, 2013

larger cloud optical thickness. Smaller cloud particles would hamper the autoconversion of cloud water into precipitation, so the presence of BB sources is expected to reduce precipitation production rate and increase cloud lifetime.

Satellite data reveal that during FMA, the SEA region exhibits the highest aerosol concentrations, it is an order of magnitude larger than that in the summer monsoon season: May-June-July-August (MJJA) season because of more BBA sources in dry FMA and less wet scavenging of aerosols compared to rainy MJJA. Accordingly, aerosol optical depth and aerosol-activated cloud particle numbers are expected to be much larger in FMA than MJJA. This is the main reason for focusing this investigation of BBA direct and indirect effects on FMA and the transition month of May. Our working hypothesis is that, high aerosol number concentration in FMA has strong influence on the radiative forcing, circulation, and precipitation of the local and surrounding region.

It has been established that aerosols influence the circulation and rainfall primarily via direct (purely radiative) and indirect (cloud microphysics modification) effects (Seinfeld and Pandis, 2006). The two effects are intrinsically interactive, and therefore their combined effects can be very different from linear sum of their effect. Even though the fundamental physics of aerosol direct and indirect effects is reasonably well understood (e.g., Seinfeld and Pandis, 2006; Sud et al., 2013), lack of aerosol data under cloudy conditions and complexities in coupling the aerosol-cloud-radiation interactions prohibits a better understanding of the impact of these processes in specific scenarios (IPCC, 2007). Besides, aerosol direct and indirect effects have not been adequately parameterized in climate models up until recently. Our current cloud physics scheme, Microphysics of clouds with Relaxed Arakawa–Schubert moist convection upgraded with prognostic Aerosol Cloud interactions (McRAS-AC; Sud et al., 2013), has indirect effect capabilities, and has been implemented in the GEOS-5 AGCM (Rienecker et al., 2008). It provides an opportunity to perform model simulation studies to systematically assess the influence of BBA on rainfall and circulation in SEA. Clearly, constrained model simulations are one plausible way to better distinguish between the roles of direct and indirect effects and their interactive influences that depend on circulation, cloud

ACPD
13, 32885–32923, 2013

types, and aerosol-dependent cloud microphysics. While in principle these effects can be properly simulated only with a coupled ocean-atmosphere model, as a first step we use an AGCM with prescribed SSTs with seasonal cycle from observations and with aerosol emission anomalies prescribed from QFED (See Sect. 2.1). In this mode, we can isolate the influence of BBA over land by comparative assessments of circulation and rainfall changes in neighboring regions. Effects of interactive SST and aerosol emissions will be considered in subsequent work.

Aerosol-cloud interaction effects on South Asia to East Asia circulation and monsoons has been the subject of some investigations with observational data analysis (Lau and Kim, 2006) as well as model simulations (Menon et al., 2002; Ramanathan et al., 2005; Lau et al., 2006; Kim et al., 2007; Meehl et al., 2008). In this endeavor, we perform a comprehensive model simulation study with the physically interactive aerosol-cloud-radiation treatment of McRAS-AC as implemented in the GEOS-5 AGCM, in order to better understand the spatiotemporal modulation of the SEA pre-monsoon season by BBA.

2 Data, model and experiments design

2.1 Datasets for aerosol effect analysis

BB is a major source of primary emissions of carbonaceous aerosols. Constrained emissions from fires are needed to model for direct and indirect effect aerosol studies. The Quick Fire Emissions Dataset (QFED, Darmenov and da Silva, 2013) was developed to meet the needs of the NASA Goddard Earth Observing System Model (GEOS) with regard to atmospheric constituent modeling and data assimilation of BB events. QFED is based on global gridded fire radiative power, derived from the MODIS Level 2 fire product. QFED is used not only as a BB inventory for the global Goddard Chemistry Aerosol Radiation and Transport (GOCART, Chin et al., 2002; Colarco et al., 2010) model in the GEOS-5 system, but also an index indicating high biomass

ACPD
13, 32885–32923, 2013

burning days for our composite analysis. Version 2.2 used in this study covers the period from January 2003 to December 2010. The QFED Level3 products are available at 0.3125° × 0.25° horizontal resolution, but are degraded to 2.5° × 2.0° for use in the present model simulation. The 1° MODIS Aqua level 3 daily product (MYD03_D3) is used for aerosol optical depth (Chu et al., 2002) and liquid cloud effective radius (Platnick et al., 2003). Data covers the period from July 2002 to present. For precipitation, 1-degree daily Global Precipitation Climatology Project (GPCP-1DD; Huffman et al., 2001) data are used covering the period October 1996 to present.

2.2 GEOS-5 AGCM with double moment microphysics and updated radiation

The numerical model used for this study is the GEOS-5 AGCM, version Fortuna 2.5 (hereafter, the baseline model) documented by Molod et al. (2012). In the current application, McRAS-AC replaces the cloud scheme of the baseline model. McRAS-AC synthesizes the initial version of McRAS (described in Sud and Walker, 1999, 2003) with subsequently developed aerosol-cloud interaction microphysics described in Sud and Lee (2007). The latest modification to McRAS-AC includes the addition of Barahona and Nenes (2009a) ice nucleation for mixed phase and ice phase clouds. The precipitation parameterization remains as before, namely Sud and Lee (2007) for the liquid phase and Sundqvist (1988) for the mixed and ice phases. In-cloud evaporation, precipitation and self-collection of cloud water are parameterized according to Sud and Lee (2007) employing a reformulated version of the Seifert and Beheng (2001, 2006) parameterization to handle the much thicker cloud-layers encountered in a coarse resolution GCM. These algorithms work seamlessly across widely varying model-layer thicknesses in the vertical. Any change in the cloud water substance mass by condensation/deposition and/or collection by precipitation works interactively through an implicit backward numerical integration that approximates the solution of the basic nonlinear coupled differential equations for the cloud source and sink terms of the mass balance tendency equation. Despite using the observationally-based Sundqvist (1988) equations for the mixed phase and ice phase precipitation tendencies, the implementa-

ACPD
13, 32885–32923, 2013

tion of Barahona and Nenes (2009a, b) ice nucleation and Bergeron–Findeisen cloud water-to-ice mass transfer (Rotstayn et al., 2000) allows a reasonable separation of cloud liquid and ice mass fractions with their respective liquid and ice particle number concentrations (LPNC and IPNC). Nevertheless, CPNC (= LPNC + IPNC) removal by precipitation is modeled as a non-linear curve-fitted relationship between cloud mass and number concentration for a prescribed Gamma distribution of cloud particle sizes. Homogenous freezing of in-cloud liquid drops surviving below −38 °C is enforced by assuming instantaneous freezing. The synthesis of the above process-modules provides an end-to-end treatment of prognostic cloud water mass (as apportioned between liquid and ice), CPNC, and precipitation tendencies. Aerosol–cloud interactions are implemented into both stratiform or large-scale clouds, and convective towers topped by detraining convective anvils that transform into large-scale clouds at a prescribed timescale of an hour. The treatment of the different cloud types can be found in several references given by Sud et al. (2013) provide a much more comprehensive discussion of McRAS-AC and its comparative performance against the cloud scheme of the baseline model.

Accurate radiation calculation is also very important for properly simulating aerosol direct/indirect effect. Our means of calculating realistic cloud radiative effect (CRE) is the advanced RRTMG radiative transfer package (Clough et al., 2005) equipped with a subcolumn generator that has been implemented in the GEOS-5 AGCM. RRTMG can be run in Monte Carlo Independent Column Approximation (McICA) mode (Pincus et al., 2003) that operate on subcolumns with either clear or completely overcast cloud layers produced by a cloud generator. Whether the cloud condensate of a particular layer is different from subcolumn to subcolumn depends on the specific assumptions about horizontal cloud heterogeneity as determined by distributions of condensate specified within the cloud generator. A prior implementation of McRAS-AC (Sud et al., 2013) used cloud water path scaling to account for the radiative effects of subgrid scale cloud water inhomogeneity. More detailed discussions about RRTMG in GEOS-5 AGCM can be found in Oreopoulos et al. (2012).

ACPD
13, 32885–32923, 2013

2.3 Experimental design

In order to investigate BBA effects on SEA climate, several observation-inspired experiments with and without BB emission over SEA are designed. Figure 1a shows the climatological amount of carbonaceous aerosol emission from BB during FMA averaged over 8 yr from 2003 to 2010, and Fig. 1b is the time series of the boxed area. The QFED dataset described earlier was used for this figure. Massive BB occurs during FMA in the east end of Cambodia, Myanmar, Laos, and Northern Thailand with peaks in March. Emissions from BB exhibit large interannual variations that apparently correlate with ENSO cycles (Tosca et al., 2010).

To isolate as much as possible the aerosol effect, the AGCM experiments were performed with climatological SST, so that large-scale forcing (e.g. El Nino) is absent. Moreover, to separate the signal from model internal variability, multi-member ensembles simulations were performed. Each simulation-set consists of a ten member ensemble covering the early January to late August period with different initial conditions. To amplify the signal of aerosol effect on climate variability, we conducted experiments with "Zero" BB emission over the green dash box region (Fig. 1a) and compared to the experiment with "High" BB emission in 2007. BB emissions outside of the boxed area and all other sources of aerosol were set to climatological means for both "High" and "Zero" emission experiments. Clearly, the differences between "High" and "Zero" emission experiments yield the effect of BB aerosol, black carbon, organic carbon, and sulfate originating from the boxed area. Properly controlled QFED emission dataset is provided to simulate GOCART in GEOS-5 system interactively.

The differences between "HighBoth" and "ZeroBoth" simulation in Table 1 are a measure of the total BB effect signals. Here, "Both" means that the model's experimental setup includes both aerosol direct and indirect effects. The indirect only simulations are identified as "HighInd" and "ZeroInd" experiments. In these simulations, we neglect the aerosol direct effect by eliminating all aerosols globally in radiative transfer calculations, allowing thus only indirect effects of aerosols to occur. "HighInd" minus "ZeroInd" dif-

ACPD
13, 32885–32923, 2013

ferences therefore measure the strength of the BB aerosol indirect effect. Finally, while not additive due to nonlinearities, comparing "Both" and "Ind" signals will give an idea about the relative contributions of direct and indirect effect to the total aerosol effect.

3 Results

3.1 Comparison between model simulations and satellite observations

Some insight on the effects of BB in SEA can be obtained by comparing high and climatological BB conditions from observational data. We have constructed composites of MODIS Aqua Level 3 daily products (MYD03_D8) for 36 days of higher BB emission index within the 2003 to 2010 period. BB emission index is time series of box-average in Fig. 1b area. Figure 2 shows comparisons between the high emission days and the 8 yr climatology of MODIS-Aqua aerosol loading for aerosol optical depth (AOD, Fig. 2a) and liquid cloud effective radius (LCER, Fig. 2b). When BB is high in FMA over inland areas of SEA compared to normal days, anomalously high AOD appears over the northern part of SEA up to the coast of Southern China. According to Lau and Kim (2013), low-level wind in the area blows from the source region to Southern China, resulting in the high BB AOD anomaly of Fig. 2a. According to the rightmost panel of Fig. 2b, the corresponding negative anomaly of liquid cloud effective radius coincides with the region where a positive AOD anomaly exists. This is a classic manifestation of aerosol indirect effect whereby increasing BB aerosol reduces the size of cloud droplets by increasing CCN number concentration. If the negative anomaly of effective radius is indeed related to aerosol, then the imprints of other aerosol indirect effects may exist in other meteorological fields as well, such as the precipitation. Figure 2c compares composited daily GPCP precipitation for the above normal BB days and the climatology. The difference plot reveals a negative precipitation anomaly over the aerosol source and adjacent area while in the vicinity of the east coast of China increased rainfall is observed. This can be interpreted in a Lagrangian framework, by the cloud holding

ACPD
13, 32885–32923, 2013

more cloud water due to reduced autoconversion efficiency as it is advected downwind and eventually releasing as precipitation far away from the source. However, since large-scale atmospheric forcing like El Nino can trigger simultaneously a reduction in precipitation and an increase in aerosols (Tosca et al., 2010) it is necessary to study in more detail shifts in the precipitation pattern from AGCM simulations.

In order to evaluate the sensitivity of the AGCM to BB aerosol variations, its output is compared to the satellite analysis. Figure 3 shows the overall BB aerosol sensitivity of the model as the difference between "HighBoth" and "ZeroBoth" experiments. Anomalies in the LCER are obtained using COSP's (http://cfmip.metoffice.com/COSP.html) MODIS simulator in GEOS-5 to enhance similarity with observations. For the ten-member ensemble mean, simulated AOD has increased downwind of the BB source, and correspondingly LCER has decreased. Not only are McRAS-AC AGCM simulations capable of simulating the response of CPNC to AOD, but the model's overall response exhibits reasonable spatial affinity with the observations, particularly on the downwind side of the BB source. For precipitation, the observations show a dipole-like anomaly pattern, namely overall decrease near source area and at eastern locations, and increase further east near coast (Fig. 2c, Diff). In the model on the other hand, the average BB signal on FMA precipitation materializes as a reduction in the precipitation of large areas south and east of the source region. Since SSTs were prescribed climatologically, no meaningful response over the ocean is expected. Potential BB aerosol effects on SEA pre-monsoon will be probed further in the following sections by taking appropriate differences of GEOS-5 experiment sets described earlier.

3.2 BB effects on cloud microphysics and precipitation simulation

One of the mechanisms that changes the nature and amount of precipitation is cloud microphysical processes as influenced by aerosols, widely known as the aerosol second indirect effect (Albrecht, 1989) what relates to precipitation efficiency. This process acts on the autoconversion rate that modulates the intensity of liquid precipitation. Our area of focus where precipitation has decreased in MODIS analysis and model simu-

ACPD
13, 32885–32923, 2013

lations is likely affected by BBA that are transported to Southern China where a persistent cloud band exists. In the model simulation the horizontal and vertical location of aerosol and the cloud band are in close proximity as seen in Fig. 4 showing the vertical cross section of BBA mixing ratio (shading) and cloud liquid water content (contour) in March obtained from the "HighBoth" experiment in the vicinity of decreased precipitation shown in Fig. 3c (105° E to 120° E). BBA are lifted aloft by topography oriented in a north to south direction, and act as an additional source of CCN in pre-existing clouds which are mostly low-level (warm) and therefore of liquid phase at this particular location and time of the year.

GOCART, aerosol module in GEOS-5 system allows for five types of aerosols, dust, sulfate, organic and black carbon, and sea salt. In the model, BB produces sulfate and carbonaceous aerosols that can be activated as cloud droplets. Sulfate aerosols are highly soluble, while simulated carbonaceous aerosols have both hydrophobic and hydrophilic modes. Hydrophilic organic and black carbon aerosols have prescribed fractions of soluble mass (0.25 and 0.1) so they also act as CCNs. Thus BBA present at the level of developing liquid clouds also activate along with the background aerosols. Under conditions of massive BB, the CCN number concentration increases greatly, and that yields increased cloud drop number concentration (CDNC) and reduced cloud droplet sizes for constant cloud water. The underlying physics leading to the reduction in LCER seems to be captured by the model (Fig. 3b). Smaller droplets reduce the efficiency of autoconversion from cloud liquid water to rain, resulting in less precipitation. The double moment microphysics in McRAS-AC enables the reduced autoconversion rate process via the parameterization below (Sud and Lee, 2007).

$$\left(\frac{\partial L_c}{\partial t}\right)_{\text{auto}} = -K L_c^4 N_c^{-2} \quad (1)$$

where L_c is the cloud liquid water content (kg m^{-3}), N_c is the CDNC (m^{-3}), and K is an accumulated constant for autoconversion (See Eq. A.2 in Sud and Lee, 2007, with units of $kg^{-3} m^3 s^{-1}$). From Eq. (1) as N_c increases under assumption of constant L_c,

ACPD
13, 32885–32923, 2013

the autoconversion rate decreases. The occurrence of this second aerosol indirect effect is confirmed by the model experiments. Monthly mean difference fields between "HighBoth" and "ZeroBoth" experiments from March to May are shown in Fig. 5 for aerosol, CDNC, cloud liquid water path (LWP), and precipitation. Plotted CDNC has been vertically averaged from 900 to 750 hPa. Red (blue) color indicates positive (negative) anomaly with increasing BB aerosol. Green contours indicate where the change by BBA is significant at the 95 % significance level, based on student's t test. Aerosols clearly increase due to BB emission with an annual peak in March, and so does the AOD anomaly. Since February is dry season for the area, the analysis focuses on March, April, and May with the latter month delineating the onset of the East Asian monsoon. With BB occurring mainly in early spring, May aerosol concentrations should not be affected much, so any signal in the meteorological fields for that month will likely be due to circulation changes induced by BB emission in the preceding months.

As mentioned earlier, as aerosol loadings increase, grid mean N_c, the product of in-cloud N_c and cloud fraction also increases. Overall, both CDNC and LWP increase for the high BB experiments, due to delayed precipitation in March and April. Still, some regions exhibit negative grid mean CDNC and LWP anomalies, possibly because of reduced cloud fraction (Fig. 6) due to reduced grid-scale relative humidity (RH) that determines cloud amount for stratiform clouds. The reduced RH is the outcome of larger stability of the lower atmosphere which suppress rising motion.

While enhanced BB emission increases aerosol loading, CCN, N_c, and even L_c, the relationship is not linear. Increased L_c eventually creates a tendency for higher autoconversion and precipitation rates which opposes the tendency of the increased N_c (Eq. 1). If we do not account for complex feedbacks, precipitation near the BB emission source can be expected to decrease if the increased N_c effect is stronger than the enhanced $L_c$effect, as shown in Fig. 5d for March and April. While the satellite data analysis suggests alternating negative-positive precipitation anomalies along the wind flow, a weak positive anomaly surrounds the simulated strong negative anomaly over Southern China in April (Fig. 5d). This may be explained by two possible mechanisms:

ACPD
13, 32885–32923, 2013

Liquid cloud water being transported far instead of precipitating out locally because of suppressed autoconversion, and reduced local precipitation creating favorable circulation conditions for precipitation downwind. Meanwhile, a statistically significant anomaly of precipitation is found in May, suggesting that large BB emission in March and April can have a delayed effect even on regions that are far away from the source. Microphysical processes may therefore not the only mechanism that reduces precipitation. The impact on May precipitation could be a combination of direct, indirect effects, and feedback processes initiated by aerosols in March-April caused anomalies in May. Further analysis of circulation changes is needed to distinguish whether this anomaly can be indeed attributed to cloud microphysics or some other mechanism, a topic that we will tackle in Sect. 3.4.

3.3 BB effects on radiation budget

BBA can change the radiation balance by both their direct and indirect effects. The direct effect of BB aerosols consists of scattering (sulfate aerosols) and absorption (black carbon aerosols) of incoming solar radiation which cause surface cooling and atmospheric heating. As discussed in Sect. 3.2, the indirect effect of BBA comes from altering cloud optical properties like LCER and cloud amount which modify the net (= shortwave + longwave) radiation budget at the top of the atmosphere (TOA), atmosphere (ATM), and surface (SFC). Figure 7 illustrates the magnitude of the net radiation change at TOA, ATM, and SFC due to both direct and indirect aerosol effects, primarily due to changes in shortwave (SW) radiation. Each map shows the monthly mean difference between "HighBoth" and "ZeroBoth" experiments from March to May with red (blue) indicating heating (cooling) anomalies by aerosol, and green contours delineating the areas of statistically significant change. The overall net radiative effect of aerosol is TOA/SFC cooling, and ATM heating near the source region, but its interpretation may require further scrutiny because contributions to net radiation change also come from circulation changes and associated feedbacks. The ATM heating provides a clearer signal of direct effects since the radiative heating comes almost exclusively

ACPD
13, 32885–32923, 2013

from aerosol absorption, while TOA and SFC cooling comes from both direct and indirect aerosol effects. In May there is little aerosol direct effect, but a significant anomaly signal exists at the TOA and SFC due to feedbacks from circulation changes. When examining TOA and SFC radiation fields in May, the dipole pattern seen near the east coast of China and Korea is due to cloud fraction change (Fig. 6) consistent with the precipitation change shown in Fig. 5d and discussed further in the following section.

Table 2 shows the differences between "HighBoth" and "ZeroBoth" experiments of the net downward (down minus up) fluxes in March when BBA peaks, regionally averaged for the emission control region. Aerosol radiative effects are much larger in the SW than the longwave (LW), so most of the net radiation change comes from SW effects. The clear sky numbers demonstrate that BB aerosol increases SW reflectance, but also absorptance, because a large fraction of BB aerosol is composed by carbonaceous aerosol which are efficient absorbers of SW radiation. Differences between cloudless and all-sky radiative flux represent the CRE change by BB aerosols which is, somewhat surprisingly, positive (weaker SW and net CRE for the "HighBoth" experiment). Despite LWP increases (Fig. 5c) and LCER decreases (Fig. 3b) in conditions of high BB, yielding an average optical thickness increases of 46 % for the cloudy part of the Table 2 region, decreased total cloud fraction due to feedbacks overrides increases cloud brightness. So, the total indirect effect including cloud feedback seems to counteract the direct aerosol effect, LCER decrease (classic "Twomey effect") and LWP increases in these GEOS-5 experiments.

3.4 Temperature, moisture, and circulation change

In this section we discuss meteorological consequences of the BB aerosol radiative effects which we have shown to lead to surface cooling and atmospheric heating. The negative surface temperature anomaly due to BB aerosol is plotted in Fig. 8 and can be seen to be very significant near the source region in March and April. Weak negative anomalies also appear in May, but are mostly insignificant statistically. The vertical profile of temperature change (black line) by BB regionally averaged from 100° E to 120° E

ACPD
13, 32885–32923, 2013

and from 18° N to 30° N (cf. red box in Fig. 8) is plotted in Fig. 9. This profile is obtained as the difference between the "HighBoth" and "ZeroBoth" experiments in March and April when the decrease of precipitation is significant, and reveals the presence of a cooling signal from the surface all the way up to 250 hPa. In order to better understand what causes the temperature change, the model's major heating/cooling rate contributions are shown in Fig. 9. The orange line shows the SW heating rate ($K\,day^{-1}$) anomaly, the red line the LW heating rate anomaly, and the blue line the anomaly of the heating rate due to the model's moist physics, namely large-scale condensation and convective processes. As expected, SW radiation heats the atmosphere near the vertical location of the aerosol layer (Fig. 4), with a peak slightly above the aerosol layer. The reason the actual temperature profile does not cross over to the positive side is other contributors to temperature change, namely LW and moist physics both of which cool the low and middle troposphere. The increase in LW cooling is a consequence of increased cloud liquid water between 800 hPa to 600 hPa due to aerosol-induced changes in microphysical processes. Although the magnitude of cooling is only about a quarter of the SW heating, it is impactful because LW cooling occurs at the exact time and location as SW heating because of liquid water and BBA collocation.

The major factor contributing to the negative temperature anomaly is the reduced moist heating, the most significant change of all the heating rate components of the model's physics. A negative moist physics heating rate anomaly translates to subdued cloud forming activity from large-scale condensation and even moist convection. In the area of interest March precipitation mostly comes from large-scale condensation, while in April there is some contribution from moist convection. The reduced convective precipitation in April, accounting for about half of the total precipitation reduction, can be explained by changes in the vertical temperature gradient. BBA direct radiative effects make the surface cooler and the 700 hPa level warmer, decreasing thus low level atmospheric instability as seen in the vertical temperature profile anomaly: even though the overall temperature change is negative (cooling), a bump of positive anomaly forms near 700 hPa that would suppress onset of moist convection.

ACPD
13, 32885–32923, 2013

Another important reason behind moist physics suppression which can explain both large-scale condensation and convective aspects is changes in atmospheric moisture. Zonally averaged moisture and meridional circulation anomalies due to BBA within 100–120° E for March, April, and 110–140° E for May are plotted in Fig. 10. The blue shading, indicating dry anomaly, spreads over the 20–30° N latitude zone where the aerosol source is located. A few factors could be making this region drier. One could be reduced surface evaporation in the region of negative surface temperature anomaly. The other could be circulation changes, specifically the substantial downward and southward flow anomalies induced by BBA. While the downward anomaly could be the result of reduced moist activity, the accompanying southward anomaly may actually be *the cause* of reduced moisture transport from low latitudes. The column-integrated moisture convergence anomaly (not shown) in the region where precipitation decreases is negative with some degree of statistical significance, albeit less than surface evaporation. Another possible cause for overall drying is the decreased precipitation itself, implying positive feedback. Because of BBA indirect effect, reduced autoconversion leaves behind more water in-cloud that advects downwind instead of being converted into local precipitation, resulting in reduced supply of moisture to the levels underneath and creating a feedback loop where smaller latent heat flux at the surface causes further decreases in precipitation.

Several mechanisms can potentially reduce precipitation in the downwind side of an active BB region. Cloud microphysics can delay the precipitation process by slowing down autoconversion, and then radiation can help make the area stable and dry, all conditions unfavorable for vigorous moist processes. As a matter of fact, dry anomalies can be involved in cloud microphysics as well through rain re-evaporation process. Likewise, a number of other variables may be changing in the same direction due to direct BBA effects on radiation and the indirect effects on cloud microphysics. For example, both effects cause SW dimming at the surface, low level drying, and decreased precipitation. Separating microphysical from radiative effects is thus a worthwhile objective which we pursue in the following section.

ACPD
13, 32885–32923, 2013

3.5 Quantitative breakdowns of direct and indirect effects

In the previous sections, all the results explaining aerosol effects were based on "High-Both" and "ZeroBoth" experiments, the first including BBA from a high emission year and the latter neglecting entirely BBA emissions from the area of strongest fire activity. The GEOS-5 AGCM accounted for both direct effects in its radiative transfer routines and indirect effects in its cloud microphysics routines. Differences between the two experiments capture both aerosol direct and indirect effects (as well as feedbacks), or in other words the combined effects (CE). In two other experimental sets, the "HighInd" and "ZeroInd" experiments, direct effects of aerosol on radiation are ignored (globally), leaving only the indirect effect (IE) of BBA to be diagnosed as the difference between the two "Ind" experiments. Our diagnostic approach to separate the direct and indirect aerosol effects of a rather complex regional climatic response consists of comparing key variables from "CE" and "IE" differences which both include feedback from circulation changes.

Table 3 shows the radiative fluxes in the same way as Table 2, but for "IE" and "CE minus IE". Evidently, CE of TOA and SFC SW fluxes and atmospheric column SW absorption are much larger than the corresponding IE of aerosols on SW. This implies a much stronger contribution of the direct effect (DE) of BBA in CE and makes sense because BBA have large optical thickness over the high emission regions. Moreover, BBA effects on radiation in the CE runs are quite similar for clear sky and all sky conditions as pointed out earlier in Sect. 3.3. This provides further evidence that IE due to BBA is an order of magnitude smaller on the SW and net radiation compared to the corresponding DE of aerosols within CE. Net radiation change by IE turns out small because it depends on cloud fraction (which does not necessarily depend on aerosols, but on cloud production, cloud dissipation, and cloud advective tendencies) and cloud optical thickness (depending upon CCN and cloud water removal tendencies by precipitation). In "ZeroInd", the (BBA-independent) cloud fraction increased while the cloud optical thickness decreased compared to "HighInd" simulations.

ACPD
13, 32885–32923, 2013

One of interesting feature of BBA signal is decreased precipitation over the downwind side of the source. The separation of "CE" and "IE" impacts on precipitation would be interesting to study for this area. To minimize feedback contributions, we can focus on variables that are primarily directly forced during the March and April timeframe and near the source region, in particular 100° E to 120° E and 18° N to 30° N. Table 4 provides the spatiotemporal averages of these CE and IE breakdowns. While the CE precipitation reduction in High minus Zero BBA is 1.08 mm day^{-1}, the corresponding IE precipitation reduction is 0.77 mm day^{-1}. For a linear system, one would attribute the 0.31 mm day^{-1} reduction corresponding to the CE minus IE difference, to the direct aerosol effect, but we are well aware that linearity is not a good assumption here, so we will view the differences to represent add-on direct effects that also contain effects of interactive circulation changes. Even though the IE averages do not show much change in the simulated surface temperature and evaporation of the boxed region, IE does have a prominent role in decreasing surface precipitation, which is caused not only by autoconversion reduction, but also by low level drying due to SW dimming in cloudy areas. In other words, the suppressed autoconversion that follows CCN and CDNC increases due to enhanced BBA activation in the IE simulations decreases precipitation, which further dries the atmosphere beneath the precipitating cloud due to reduced evaporation of rain. In comparison, the DE part of CE has a more straightforward effect on the moisture supply that can be traced to atmospheric stabilization and reduced surface temperature due to surface cooling. So while both CE and IE tend to reduce precipitation, the mechanisms overall can differ even if they share the common processes of slower autoconversion and low level drying.

4 Summary and discussion

An aerosol impact study including both the direct and indirect effects focusing on Southeast Asia pre-monsoon season is conducted based on simulations using the GEOS-5 AGCM with double moment cloud microphysics called McRAS-AC, interactive GO-

ACPD
13, 32885–32923, 2013

CART aerosol model, advanced radiative transfer package RRTMG applying the Monte Carlo Independent Column Approximation, and CFMIP Observation Simulator Package (COSP). Analysis of GEOS-5 integrations with and without biomass burning (BB) emission allows us to separate the responses of clouds and precipitation to aerosol from those due to dynamics and meteorological fields. Our analysis indicates that plausible reasons for the reduced precipitation are (a) vertical stabilization by atmospheric heating aloft accompanied by surface cooling due to the absorptive nature of the BB aerosols; (b) less efficient autoconversion despite liquid water increases due to increased cloud droplet number concentration; and (c) suppressed moist processes due to lower atmospheric drying. With properly designed experiments we managed to separate the impacts of direct and indirect effects. While vertical stabilization is traced to direct aerosol-radiation interaction which causes rapid cloud adjustments (commonly referred to as the "semi-direct effect") because of depressed convective activity, and the reduced autoconversion rate is primarily a consequence of aerosol-cloud interaction (the indirect effect), the drying of the lower and middle troposphere is caused by both.

An interesting, and somewhat unexpected, phenomenon induced by BB aerosols is the May precipitation anomaly near the Korean peninsula shown in Fig. 5d. Since BB is not a major factor in May aerosol loadings, the precipitation anomaly could be due to circulation changes triggered by BB in the preceding month. In March and April, the surface temperature over Southeast Asia drops significantly due to the combined direct and indirect solar dimming effect of BB aerosols and this reduces the meridional temperature gradient. Figure 10 shows that the overall circulation anomaly heads south in March and April. The May circulation anomaly exhibits downward motion at 30° N and a little upward motion south of 30° N. According to Kim et al. (2007) an upper level jet stream change can induce secondary circulation changes near the entrance of the jet core in East Asia. In their analysis, an initial surface cooling by sulfate aerosol direct effect resulted in a reduced north–south thermal gradient. Figure 11a shows a similar weakened meridional temperature gradient change by surface cooling during March

ACPD
13, 32885–32923, 2013

and April. This reduced gradient weakens the zonal wind shear through the thermal wind relationship, and slows down the westerly jet stream (Fig. 11b). The deceleration causes ageostrophic meridional winds and, in this case, anomalous sinking motion at 30° N (see Fig. 10, May), conditions that are less favorable for precipitation. Although Kim et al. (2007) account only for direct forcing of aerosol, the circulation anomalies induced by the BB aerosol emissions of this study are similar, because indirect effects do not induce much surface forcing in this experiments.

While this study provided some confirmation that our BB sensitivity in the model looks similar to that from MODIS analysis, the "Zero" biomass burning assumption is admittedly extreme. So the real meteorological signal by biomass burning aerosol could be weaker than suggested by the results shown here. But given the plausibility of how the model's mechanisms operate, there is good possibility that real conditions would be consistent with the overall tendencies of the model. Still, there is much room for further development of the GEOS-5 model towards more realism. For example, in the current convective parameterization aerosols always suppress convection. Phenomena such as aerosol-induced convective invigoration (Rosenfeld et al., 2008) can therefore not be reproduced because heat release due to freezing at high altitude does not affect the convective mass flux. This process could probably be better represented in a bulk mass flux convection scheme (e.g., Kim and Kang, 2012), but it remains to be seen whether its inclusion in such a scheme would ultimately affect overall convective activity in a substantial way. Our method of separating direct and indirect aerosol effects may be imperfect, but no better alternative currently exists given present modeling limitations. Nevertheless, we believe that this study provides a foundation on which to develop better methodologies to properly distinguish direct and indirect effect sensitivity to aerosols in large-scale models.

Acknowledgements. Funding from NASA's Modeling Analysis and Prediction (MAP) program managed by David Considine, and from the Interdisciplinary Research in Earth Science (IDS) program (Water and Energy Cycle Impacts of Biomass Burning subelement) managed by Hal Maring is gratefully acknowledged.

ACPD
13, 32885–32923, 2013

References

Albrecht, B.: Aerosols, cloud microphysics, and fractional cloudiness, Science, 245, 1227–1230, doi:10.1126/science.245.4923.1227, 1989.

Barahona, D. and Nenes, A.: Parameterizing the competition between homogeneous and heterogeneous freezing in cirrus cloud formation – monodisperse ice nuclei, Atmos. Chem. Phys., 9, 369–381, doi:10.5194/acp-9-369-2009, 2009a.

Barahona, D. and Nenes, A.: Parameterizing the competition between homogeneous and heterogeneous freezing in ice cloud formation – polydisperse ice nuclei, Atmos. Chem. Phys., 9, 5933–5948, doi:10.5194/acp-9-5933-2009, 2009b.

Chin, M., Ginoux, P., Kinne, S., Torres, O., Holben, B., Duncan, B., Martin, R., Logan, J., Higurashi, A., and Nakajima, T.: Tropospheric aerosol optical thickness from the GOCART model and comparisons with satellite and Sun photometer measurements, J. Atmos. Sci., 59, 461–483, doi:10.1175/1520-0469(2002)059<0461:TAOTFT>2.0.CO;2, 2002.

Chu, D., Kaufman, Y., Ichoku, C., Remer, L., Tanre, D., and Holben, B.: Validation of MODIS aerosol optical depth retrieval over land, Geophys. Res. Lett., 29, doi:10.1029/2001GL013205, 2002.

Clough, S., Shephard, M., Mlawer, E., Delamere, J., Iacono, M., Cady-Pereira, K., Boukabara, S., and Brown, P.: Atmospheric radiative transfer modeling: a summary of the AER codes, J. Quant. Spectrosc. Ra., 91, 233–244, doi:10.1016/j.jqsrt.2004.05.058, 2005.

Colarco, P., da Silva, A., Chin, M., and Diehl, T.: Online simulations of global aerosol distributions in the NASA GEOS-4 model and comparisons to satellite and ground-based aerosol optical depth, J. Geophys. Res.-Atmos., 115, D14207, doi:10.1029/2009JD012820, 2010.

Darmenov, A. and da Silva, A.: The Quick Fire Emissions Dataset (QFED) – Documentation of Versions 2.1, 2.2 and 2.4., NASA Technical Report Series on Global Modeling and Data Assimilation. NASA TM-2013-104606, vol. 32, 183 pp., 2013.

Gautam, R., Hsu, N., Eck, T., Holben, B., Janjai, S., Jantarach, T., Tsay, S., and Lau, W.: Characterization of aerosols over the Indochina peninsula from satellite-surface observations during biomass burning pre-monsoon season, Atmos. Environ., 78, 51–59, doi:10.1016/j.atmosenv.2012.05.038, 2013.

Huffman, G., Adler, R., Morrissey, M., Bolvin, D., Curtis, S., Joyce, R., McGavock, B., and Susskind, J.: Global precipitation at one-degree daily resolution

ACPD
13, 32885–32923, 2013

from multisatellite observations, J. Hydrometeorol., 2, 36–50, doi:10.1175/1525-7541(2001)002<0036:GPAODD>2.0.CO;2, 2001.
IPCC: Climate Change, The Physical Science Basis, Contribution of Working Group I to the Fourth Assessment Report of the Intergovernmental Panelon Climate Change, edited by: Solomon, S. et al., Cambridge Univ. Press, USA, 2007.
Kim, D. and Kang, I.-S.: A bulk mass flux convection scheme for climate model: description and moisture sensitivity, Clim. Dynam., 38, 411–429, doi:10.1007/s00382-010-0972-2, 2012.
Kim, M.-K., Lau, K.-M., Kim, K.-M., and Lee, W.: A GCM study of effects of radiative forcing of sulfate aerosol on large scale circulation and rainfall in East Asia during boreal spring, Geophys. Res. Lett., 34, L24701, doi:10.1029/2007GL031683, 2007.
Lau, K.-M. and Kim, K.-M.: Observational relationships between aerosol and Asian monsoon rainfall, and circulation, Geophys. Res. Lett., 33, L21810, doi:10.1029/2006GL027546, 2006.
Lau, K.-M. and Kim, K.-M.: Impact of aerosols on the Asian monsoon – an interim assessment, in: Climate Change: Multidecadal and Beyond, edited by: Chang, C.-P., Ghil, M., Latif, M., and Wallace, M., in press, Springer Praxis, Berlin Heidelberg, 2013.
Lau, K.-M., Kim, M.-K., and Kim, K.-M.: Asian summer monsoon anomalies induced by aerosol direct forcing: the role of the Tibetan Plateau, Clim. Dynam., 26, 855–864, doi:10.1007/s00382-006-0114-z, 2006.
Li, G., Lei, W., Bei, N., and Molina, L. T.: Contribution of garbage burning to chloride and $PM_{2.5}$ in Mexico City, Atmos. Chem. Phys., 12, 8751–8761, doi:10.5194/acp-12-8751-2012, 2012.
Meehl, G., Arblaster, J., and Collins, W.: Effects of black carbon aerosols on the Indian monsoon, J. Climate, 21, 2869–2882, doi:10.1175/2007JCLI1777.1, 2008.
Menon, S., Hansen, J., Nazarenko, L., and Luo, Y.: Climate effects of black carbon aerosols in China and India, Science, 297, 2250–2253, doi:10.1126/science.1075159, 2002.
Molod, A., Takacs, L., Suarez, M. J., Bacmeister, J., Song, I.-S., and Eichmann, A.: GEOS-5 atmospheric general circulation model: mean climate development from MERRA to Fortuna, Tech. Memo., NASA Goddard Space Flight Center, MD, 115 pp., 2012.
Moorthy, K., Babu, S., Manoj, M., and Satheesh, S.: Buildup of aerosols over the Indian Region, Geophys. Res. Lett., 40, 1011–1014, doi:10.1002/grl.50165, 2013.
Oreopoulos, L., Lee, D., Sud, Y. C., and Suarez, M. J.: Radiative impacts of cloud heterogeneity and overlap in an atmospheric General Circulation Model, Atmos. Chem. Phys., 12, 9097–9111, doi:10.5194/acp-12-9097-2012, 2012.

ACPD
13, 32885–32923, 2013

Pincus, R., Barker, H., and Morcrette, J.: A fast, flexible, approximate technique for computing radiative transfer in inhomogeneous cloud fields, J. Geophys. Res.-Atmos., 108, 4376, doi:10.1029/2002JD003322, 2003.

Platnick, S., King, M., Ackerman, S., Menzel, W., Baum, B., Riedi, J., and Frey, R.: The MODIS cloud products: algorithms and examples from Terra, IEEE T. Geosci. Remote, 41, 459–473, doi:10.1109/TGRS.2002.808301, 2003.

Ramanathan, V., Chung, C., Kim, D., Bettge, T., Buja, L., Kiehl, J., Washington, W., Fu, Q., Sikka, D., and Wild, M.: Atmospheric brown clouds: impacts on South Asian climate and hydrological cycle, P. Natl. Acad. Sci. USA, 102, 5326–5333, doi:10.1073/pnas.0500656102, 2005.

Rienecker, M. M., Suarez, M. J., Todling, R., Bacmeister, J., Takacs, L., Liu, H.-C., Gu, W., Sienkiewicz, M., Koster, R. D., Gelaro, R., Stajner, I., and Nielsen, J. E.: The GEOS-5 Data Assimilation System Documentation of Versions 1 5.0.1, 5.1.0, and 5.2.0. NASA/TM–2008–2 104606, vol. 27, 118 pp., 2008.

Roelofs, G.-J.: A steady-state analysis of the temperature responses of water vapor and aerosol lifetimes, Atmos. Chem. Phys., 13, 8245–8254, doi:10.5194/acp-13-8245-2013, 2013.

Rosenfeld, D., Lohmann, U., Raga, G., O'Dowd, C., Kulmala, M., Fuzzi, S., Reissell, A., and Andreae, M.: Flood or drought: how do aerosols affect precipitation?, Science, 321, 1309–1313, doi:10.1126/science.1160606, 2008.

Rotstayn, L., Ryan, B., and Katzfey, J.: A scheme for calculation of the liquid fraction in mixed-phase stratiform clouds in large-scale models, Mon. Weather Rev., 128, 1070–1088, doi:10.1175/1520-0493(2000)128<1070:ASFCOT>2.0.CO;2, 2000.

Seifert, A. and Beheng, K.: A double-moment parameterization for simulating autoconversion, accretion and selfcollection, Atmos. Res., 59, 265–281, doi:10.1016/S0169-8095(01)00126-0, 2001.

Seifert, A. and Beheng, K.: A two-moment cloud microphysics parameterization for mixed-phase clouds. Part 1: Model description, Meteorol. Atmos. Phys., 92, 45–66, doi:10.1007/s00703-005-0112-4, 2006.

Seinfeld, J. H. and Pandis, S. N.: Atmospherical Chemistry and Physics – from Air Pollution to Climate Change, 2nd edn., John Wiley & Sons, 987 pp., 2006.

Sud, Y. C. and Lee, D.: Parameterization of aerosol indirect effect to complement McRAS cloud scheme and its evaluation with the 3-year ARM-SGP analyzed data for single column models, Atmos. Res., 86, 105–125, doi:10.1016/j.atmosres.2007.03.007, 2007.

ACPD
13, 32885–32923, 2013

Sud, Y. C. and Walker, G.: Microphysics of clouds with the relaxed Arakawa–Schubert scheme (McRAS). Part I: Design and evaluation with GATE Phase III data, J. Atmos. Sci., 56, 3196–3220, 1999.

Sud, Y. C. and Walker, G.: New upgrades to the microphysics and thermodynamics of clouds in McRAS: SCM and GCM evaluation of simulation biases in GEOS GCM, Proceedings of the Indian National Science Academy Part-A Physical Sciences, 69, 543–565, 2003.

Sud, Y. C., Lee, D., Oreopoulos, L., Barahona, D., Nenes, A., and Suarez, M. J.: Performance of McRAS-AC in the GEOS-5 AGCM: aerosol-cloud-microphysics, precipitation, cloud radiative effects, and circulation, Geosci. Model Dev., 6, 57–79, doi:10.5194/gmd-6-57-2013, 2013.

Sundqvist, H.: Parameterization of condensation and associated clouds in models for weather prediction and general circulation simulation, in: Physically Based Modeling and Simulation of Climate and Climatic Change, edited by: Schlesinger, M. E., Kluwer Academic Publishers, Dordrecht, the Netherlands, 433–461, 1988.

Taylor, D.: Biomass burning, humans and climate change in Southeast Asia, Biodivers. Conserv., 19, 1025–1042, doi:10.1007/s10531-009-9756-6, 2010.

Tosca, M. G., Randerson, J. T., Zender, C. S., Flanner, M. G., and Rasch, P. J.: Do biomass burning aerosols intensify drought in equatorial Asia during El Niño?, Atmos. Chem. Phys., 10, 3515–3528, doi:10.5194/acp-10-3515-2010, 2010.

Twomey, S.: The influence of pollution on the shortwave albedo of clouds, J. Atmos. Sci., 34, 1149–1152, 1977.

Wiedinmyer, C., Akagi, S. K., Yokelson, R. J., Emmons, L. K., Al-Saadi, J. A., Orlando, J. J., and Soja, A. J.: The Fire INventory from NCAR (FINN): a high resolution global model to estimate the emissions from open burning, Geosci. Model Dev., 4, 625–641, doi:10.5194/gmd-4-625-2011, 2011.

ACPD
13, 32885–32923, 2013

Table 1. Experimental designs for our GEOS-5 AGCM simulations. "Zero" stands for zero BB emission over the green dash box region of Fig. 1a, "High" for high (year 2007, Fig. 1b) emission. Symbols under aerosol direct effect (ADE) and aerosol indirect effect (AIE) indicate experiments with (O) and without (X) the effect.

	BB	ADE	AIE
HighBoth	High	O	O
ZeroBoth	Zero	O	O
HighInd	High	X	O
ZeroInd	Zero	X	O

ACPD
13, 32885–32923, 2013

Table 2. Radiative flux change ($W m^{-2}$) by BB aerosol: Numbers indicate the difference between HighBoth and ZeroBoth experiments on Mar and Apr, regional averaged from 90° E to110° E and from 12° N to 30° N only including land grid (emission control region). All fluxes are net downward, which means upward fluxes are subtracted from downward fluxes.

	TOA	ATM	SFC
SW, all sky	−9.5	15.1	−24.6
SW, clear sky	−9.0	17.1	−26.1
LW, all sky	0.3	−2.5	2.8
LW, clear sky	1.2	−1.0	2.2

ACPD
13, 32885–32923, 2013

Table 3. Radiative flux change ($W m^{-2}$) by indirect effect of BB aerosol, and the differences from Table 2. "IE" indicates the difference between HighInd and ZeroInd experiments, while others are the same as Table 2.

	TOA		ATM		SFC	
	IE	CE–IE	IE	CE–IE	IE	CE–IE
SW, all sky	0.5	−10	0.0	15.1	0.5	−25.1
SW, clear sky	−0.3	−8.7	−0.3	17.4	0.0	−26.1
LW, all sky	−2.1	2.4	0.8	−3.3	−1.3	4.1
LW, clear sky	−0.4	1.6	0.7	−1.7	−1.1	3.3

ACPD
13, 32885–32923, 2013

Table 4. Analysis of combined effects (CE, Direct + Indirect) and only indirect effect (IE). [a] Regional average from 100° E to 120° E and 18° N to 30° N, on Mar and Apr, and [b] 975 hPa to 500 hPa vertical.

Aerosol Effect	Combined effect	Indirect effect
Precipitation[a] (mm day^{-1})	−1.08	−0.77
Surface temperature[a] (K)	−0.59	0.09
Surface evaporation[a] (mm day^{-1})	−0.25	0.07
Moisture[b] (g kg^{-1})	−0.38	−0.23
Moist heating rate[b] (K day^{-1})	−0.29	−0.16
Temperature[b] (K)	−0.24	−0.07

ACPD
13, 32885–32923, 2013

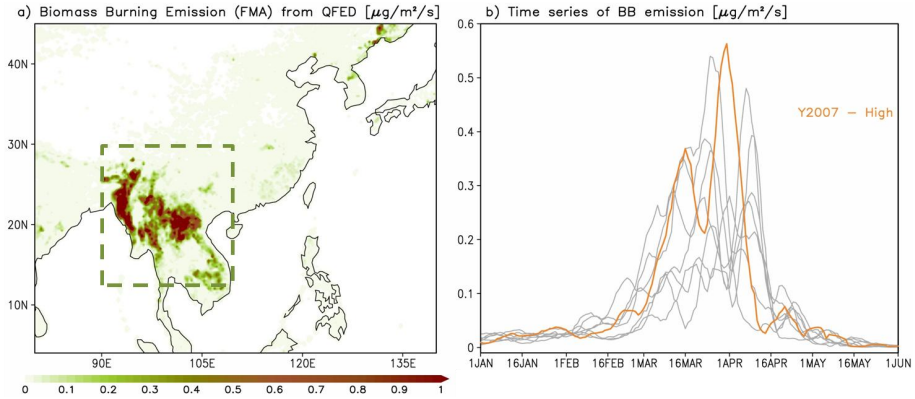

Fig. 1. QFED BB emission data (OC data is used for this figure, unit of $\mu g\,m^{-2}\,s^{-1}$). **(a)** February-March-April mean and **(b)** averaged time series for dashed box area. Time series are smoothed by a seven-day moving average. Orange line represents data for year 2007 for high BB simulation experiments. Other years are plotted in gray.

ACPD
13, 32885–32923, 2013

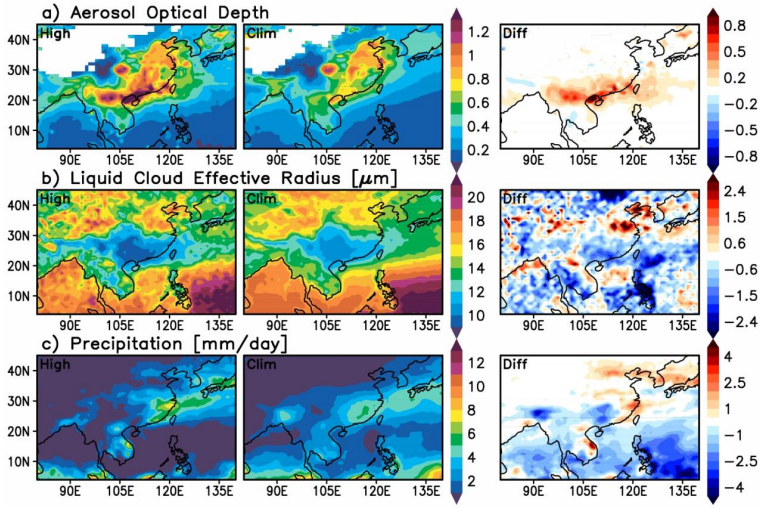

Fig. 2. Composite analysis and differences (Diff) in **(a)** aerosol optical depth and **(b)** liquid cloud effective radius (μm) from MODIS-Aqua retrievals, and **(c)** GPCP precipitation (mm day^{-1}). High emission (left), climatology (middle) and differences: high minus climatology (right) panels respectively. Here 36 high emission days and 8 yr climatology data are used.

ACPD
13, 32885–32923, 2013

Influences of aerosols on pre-monsoon circulation

D. Lee et al.

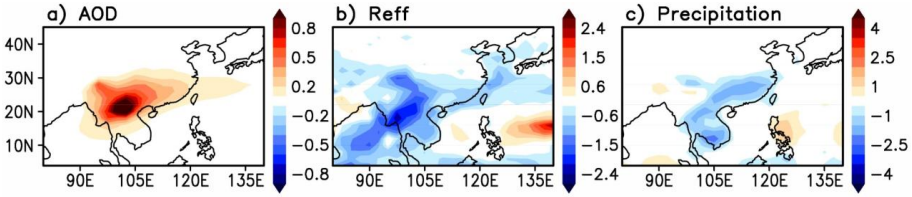

Fig. 3. Same variables as in Fig. 2 but for HighBoth minus ZeroBoth differences of AGCM simulations. Panels show **(a)** aerosol optical depth, **(b)** liquid cloud effective radius (μm) and precipitation rate (mm day^{-1}) during the FMA time period.

ACPD
13, 32885–32923, 2013

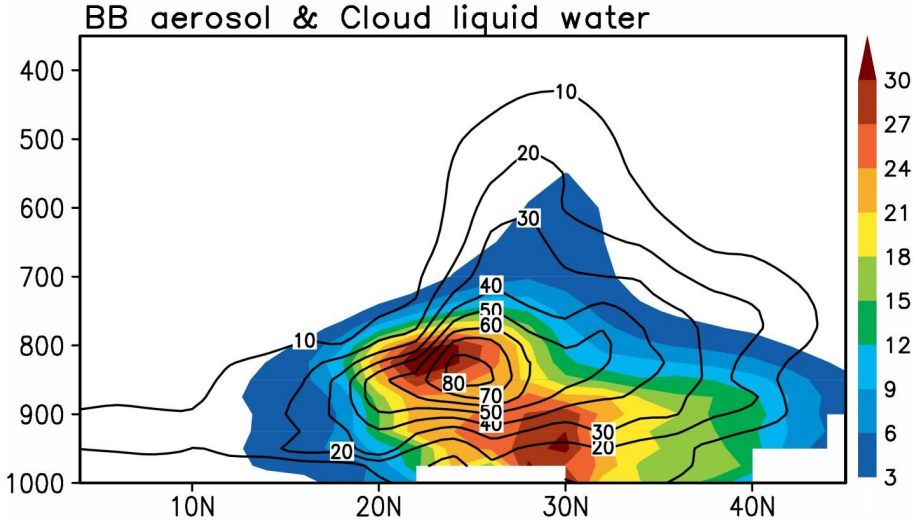

Fig. 4. Vertical cross section of simulated mixing ratio of BB aerosol (shading, $\mu g\,kg^{-1}$) and cloud liquid water (contour, $mg\,kg^{-1}$) in March in HighBoth simulations; zonal averaging is performed for 105 to 120° E.

ACPD
13, 32885–32923, 2013

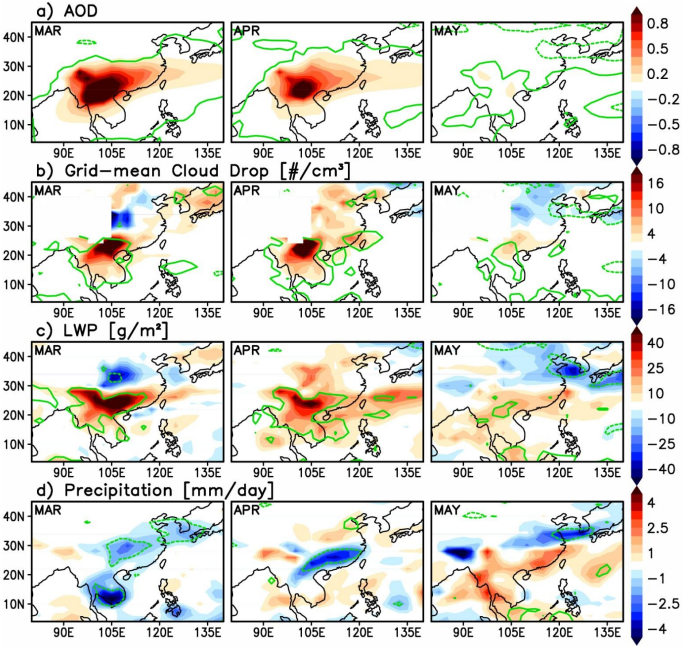

Fig. 5. HighBoth minus ZeroBoth for FMA simulations representing BBA effects on **(a)** aerosol optical depth, **(b)** grid mean cloud drop number concentration, **(c)** liquid water path (LWP), and **(d)** precipitation. Green contour mark regions of > 95 % significant in a student's *t* test.

ACPD
13, 32885–32923, 2013

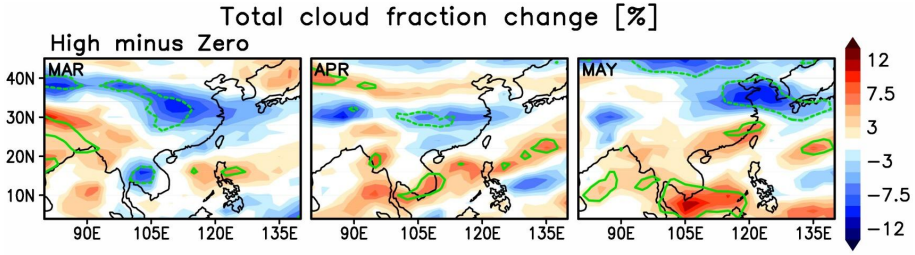

Fig. 6. Same layout as in Fig. 5, but for total cloud fraction (%) from COSP.

ACPD
13, 32885–32923, 2013

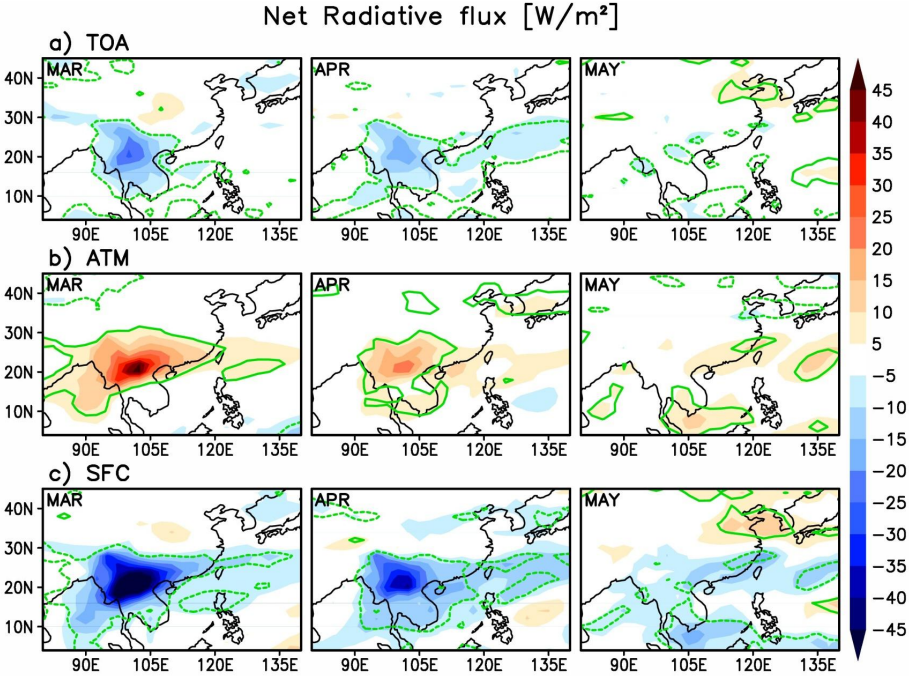

Fig. 7. Same layout as in Fig. 5, but for net radiative fluxes at **(a)** top of the atmosphere, **(b)** column atmosphere, and **(c)** surface.

ACPD
13, 32885–32923, 2013

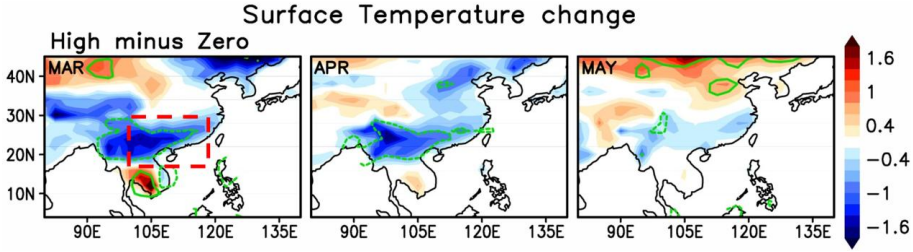

Fig. 8. Same layout as in Fig. 5, but for surface temperature. Red dashed domain is for area average fields in Fig. 9 and Table 4.

ACPD
13, 32885–32923, 2013

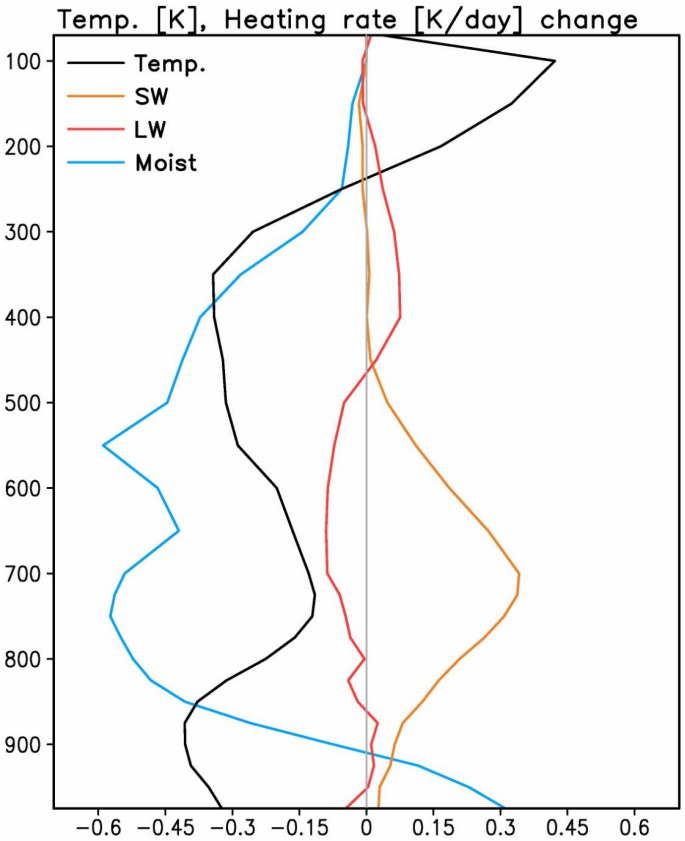

Fig. 9. Vertical profile of temperature (K) and heating rate ($K\,day^{-1}$) differences between High-Both and ZeroBoth simulations for March and April when decrease of precipitation is significant, averaging region 100° E to 120° E and 18° N to 30° N is marked in Fig. 8. Black, orange, red and blue lines represent temperature, SW heating rate, LW heating rate, and the heating rate due to the model's moist physics.

ACPD
13, 32885–32923, 2013

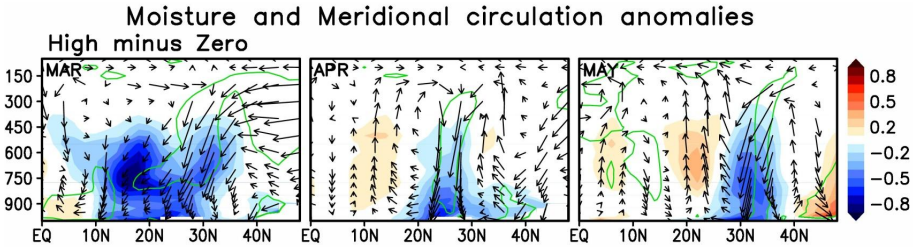

Fig. 10. Zonally-averaged profiles of moisture (shading) and meridional circulation anomalies (vectors, horizontal component is for meridional wind anomaly, vertical component is for pressure velocity) from HighBoth minus ZeroBoth experiments over the longitude sector 100–120° E for March, April and sector 110–140° E for May. Units of pressure velocity, meridional wind, and water vapor mixing ratio are 10^{-2} Pa s^{-1}, m s^{-1}, and g kg^{-1} respectively.

ACPD
13, 32885–32923, 2013

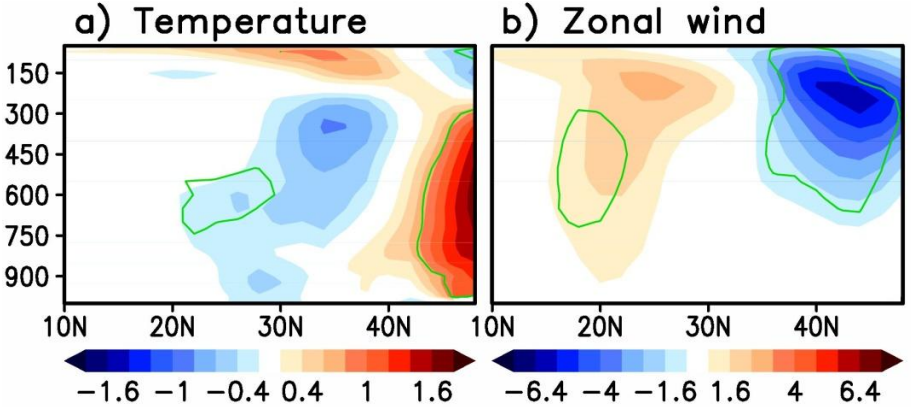

Fig. 11. Zonal mean temperature (K) and wind ($m\,s^{-1}$) differences between HighBoth and Zero Both BBA for 110–140° E in May. Green contour identifies regions with > 95 % significant differences according to student's *t* test.

ACPD
13, 32885–32923, 2013